Lysine 27 dimethylation of *Drosophila* linker histone dH1 contributes to heterochromatin organization independently of H3K9 methylation

Jordi Bernués [1,2,*], Andrea Izquierdo-Boulstridge[1,2], Oscar Reina[2], Lucía Castejón[1,2], Elena Fernández-Castañer[1], Núria Leal[1], Nancy Guerrero-Pepinosa[1], Carles Bonet-Costa[1,2], Olivera Vujatovic[1,2], Paula Climent-Cantó[1,2] and Fernando Azorín [1,2]

[1]Institute of Molecular Biology of Barcelona, IBMB, CSIC, Baldiri Reixac 4, 08028 Barcelona, Spain and [2]Institute for Research in Biomedicine of Barcelona, IRB Barcelona. The Barcelona Institute of Science and Technology. Baldiri Reixac 10, 08028 Barcelona, Spain

ABSTRACT

Post-translational modifications (PTMs) of core histones are important epigenetic determinants that correlate with functional chromatin states. However, despite multiple linker histone H1s PTMs have been identified, little is known about their genomic distribution and contribution to the epigenetic regulation of chromatin. Here, we address this question in *Drosophila* that encodes a single somatic linker histone, dH1. We previously reported that dH1 is dimethylated at K27 (dH1K27me2). Here, we show that dH1K27me2 is a major PTM of *Drosophila* heterochromatin. At mitosis, dH1K27me2 accumulates at pericentromeric heterochromatin, while, in interphase, it is also detected at intercalary heterochromatin. ChIPseq experiments show that >98% of dH1K27me2 enriched regions map to heterochromatic repetitive DNA elements, including transposable elements, simple DNA repeats and satellite DNAs. Moreover, expression of a mutated dH1K27A form, which impairs dH1K27me2, alters heterochromatin organization, upregulates expression of heterochromatic transposable elements and results in the accumulation of RNA:DNA hybrids (R-loops) in heterochromatin, without affecting H3K9 methylation and HP1a binding. The pattern of dH1K27me2 is H3K9 methylation independent, as it is equally detected in flies carrying a H3K9R mutation, and is not affected by depletion of Su(var)3–9, HP1a or Su(var)4–20. Altogether these results suggest that dH1K27me2 contributes to heterochromatin organization independently of H3K9 methylation.

INTRODUCTION

The eukaryotic genome is structured in the form of chromatin, which is built up by the monotonous repetition of a fundamental unit, the nucleosome. Nucleosomes are formed by about 147 bp of DNA wrapped around a protein core particle formed by two copies of each of the core histones (H2A, H2B, H3 and H4). Onto this elemental unit a fifth linker histone H1 binds at the entry/exit point of the DNA, interacting with an additional 15–50 bp DNA fragment (reviewed in (1)). Core histones are subjected to a plethora of post-translational modifications (PTMs) that affect nucleosome structure and function in an epigenetic way (reviewed in (2)). In this regard, several functional chromatin states have been described on the basis of specific core histones PTMs and chromatin associated proteins (3,4). In particular, the silent gene-poor heterochromatic regions are enriched in H3K9me2/3 and H4K20me3, and in Heterochromatin Protein 1a (HP1a). As a matter of fact, a main pathway for heterochromatin formation involves H3K9 methylation by the histone methyl-transferase (HMT) Su(var)3–9 and subsequent binding of HP1a (reviewed in (5)) that, in its turn, mediates recruitment of the Su(var)4–20 HMT that methylates H4K20 (6,7). However, it is appealing how so little is known about linker histones H1 PTMs and their potential contribution to functional epigenetic states (8).

Histone H1 is usually present in multiple isoforms in vertebrates (up to 11 in mouse and human) subdivided into somatic and germline variants (reviewed in (9)). In *Drosophila*, there is only one somatic variant (dH1), which is encoded by a multigene family of ~100 copies located in the histone *locus*, and a second single-copy germline variant (Big H1) (10,11). All isoforms present a similar structure containing N- and C-terminal unstructured tails, and a central globular domain. In mice tissues and in human MCF7 and HeLa

*To whom correspondence should be addressed. Tel: +34 934034960; Email: jbmbmc@ibmb.csic.es

cells, many PTMs have been identified in the somatic H1 isoforms including phosphorylation of S and T, and acetylation, formylation, methylation and ubiquitylation of K (12). Additionally, di-methylation of K and methylation of R were also described in mice (12). Notably, in both species these PTMs were present all along the H1 sequence (not restricted to the N- and C-terminal tails) and all isoforms were shown to bear many PTMs (12). However, their genomic distribution and functional relevance remain largely unknown. Similarly, in *Drosophila*, there is abundant information on core histones PTMs but little information on linker histones PTMs (8). In this regard*,* multiple PTMs were reported in somatic dH1 in Schneider S2 cells (13). Amongst them, dimethylation of lysine 27 (dH1K27me2) in the N-terminal tail was identified. Here, this modification is further characterized. We show that dH1K27me2 is a major PTM of *Drosophila* heterochromatin that contributes to its structural and functional organization independently of the Su(var)3–9/HP1a pathway for heterochromatin formation.

MATERIALS AND METHODS

Fly stocks and antibodies

UAS-dH1::GFP and UAS-dH1K27A::GFP stocks were prepared by inserting the corresponding ORFs (WT or carrying a K27A mutation generated by PCR) into pEGFP (Clontech) to generate fusion proteins and then the inserts were cloned into pUAST (details can be provided on request). Constructs were injected into *Drosophila* w^{1118} embryos and transgenic flies were obtained. H2AvD2::GFP flies were kindly provided by Dr Saint (14). yw; ΔHisC, 2xUAS-YFP; 12xHWT and yw; ΔHisC, 2xUAS-YFP; 12xK9R flies were kindly provided by Dr Duronio (15). *Nub*-GAL4; UAS-Dic2 was kindly provided by Dr Casali and are described in Bloomington Stock center. w^{1118}, *Da*-GAL4 (BL55849), Act-GAL4 (BL-8760), UAS-Su(var)4–20^{RNAi} (BL-32892) and UAS-KDM4B(EP)/CyO (BL20208) fly stocks were obtained from Bloomington stock Center. UAS-HP1a^{RNAi}(V31995), UAS-Su(var)3–9^{RNAi} (V101494), UAS-Egg^{RNAi} (SETDB1; V101677 and V33730), UAS-G9a^{RNAi} (V110662 and V25474), UAS-E(z)^{RNAi} (V33659, V27993 and V31617), UAS-KDM4A^{RNAi} (V32650, V107868 and V32652), and UAS-KDM4B^{RNAi} (V110158), were obtained from VDRC (Vienna). UAS-LID^{RNAi} (9088R1 and 9088R2) were obtained from NIG-FLY. KDM4A(EP) (KG04636) was provided by Dr Workman. UAS-KDM4AFlag/CyO was previously described (16).

Rabbit αdH1, a generous gift of Dr Kadonaga, was raised against endogenous dH1 purified from embryos and is characterized in (17,18). Rabbit αdH127me2 is described in (13)), rat αHP1a is described in (19)) and monoclonal S9.6 antibody is described in (20). All other antibodies were commercially available: mouse αGFP (Roche, 11814 460 001), rabbit αGFP (Life technologies, A11122), rabbit αH3K9me2 (Millipore, 07-441), and rabbit αH4K20me3 (Abcam, Ab9053). Secondary antibodies conjugated to Cyanine 2, 3 and 5 and to HRP were from Jackson.

Western blot (WB) and peptide dot-blot assays

WB and peptide dot-blot assays were performed as described in (13). Custom designed *Drosophila* peptides for dot blot assays were: dH1K27unmod (CKKVVQKKAS GSAGT) and dH1K27me2 (CKKVVQ[2Me-K]KASGSA GT) were obtained from Caslo (Denmark), and H3K9me3 (residues 1–21) was from Upstate-Millipore. For WB, total extracts were prepared in 100 μL SDS-PAGE protein loading buffer (PLB) from 30–50 salivary glands. Additionally, H1-enriched extracts were also prepared (from either ∼100 μL of staged embryos; from salivary glands, brains and imaginal disks from 30 to 50 larvae, and abdomens and heads from 10 to 20 adult flies) by 5% perchloric acid extraction for 1h at 4°C with rotation. Extracts were spun for 5 min at 20 000 × g at 4°C, supernatants were recovered and material containing linker histone H1 was precipitated by addition of trichloroacetic acid up to 20% and 10 min spinning as above. Pellets were washed once with cold acetone/1 M HCl (9:1 v/v) and twice with pure acetone. Pellets were allowed to dry completely at room temperature and finally they were resuspended in PLB. WB analysis of larvae expressing dH1::GFP or dH1K27A::GFP were similarly performed using total salivary glands extracts (from at least 50 larvae) from UAS-dH1::GFP and UAS-dH1K27A::GFP flies crossed with several GAL drivers. Antibodies used were: αdH1K27me2 (1:2000), αdH1 (1:20000), αGFP (1:2000), αH4 (1:1000), αH3K9me2 (1:1000), and αHP1a (1:10 000). Secondary HRP-conjugated antibodies were always used at 1:10 000 (Jackson) and developed with ECL (G&E biochemicals).

Immunostaining experiments

Drosophila cell lines S2 and Kc167 were grown under standard conditions in Schneider's medium supplemented with 10% fetal calf serum at 25°C. For metaphase chromosomes preparation 5 mL-flasks were grown to 3×10^6 cells/mL. Then 240 μl of Colcemid (Roche, at 10 μg/mL) were added and incubated for 6 h at 25°C. 300 μL of cells from above were added to 1 mL of hypotonic buffer (IMAC: 50 mM glycerol, 5 mM KCl, 10 mM NaCl, 0,8 mM $CaCl_2$, 10 mM sucrose) and incubated for 5 min. This cell suspension was impacted (200 μL) on slides using a Cytospin at 500 rpm for 10 min at room temperature. Slides were allowed to dry at room temperature for 1 h and fixed in 4% *p*-formaldehyde (10 min), washed in PBS and then in PBS-T (PBS, 0.2% Tween 20, 0.1% BSA). Then αdH1K27me2 (1:200) or αdH1 (1:4000) in PBS-T was added and incubated 1h in a dark moist chamber at room temperature, washed with PBS-T and then treated with secondary α-rabbit-Cy3 antibody (1:400 in PBS-T) for 45 min. After washing with PBS-T and PBS, samples were mounted in MOWIOL-0.2 ng/μL DAPI and visualized on a Leica SPE confocal microscope.

For neuroblast preparation, 3–5 brains were dissected in 0.7% NaCl and washed twice in the same solution. Brains were incubated at room temperature with 100 μL Colcemid (at 10 μg/mL with 0.7% NaCl) in a dark moist chamber for 2 h. After washing in PBS, they were treated with 0.54 mL of dissociation buffer (0.8% Na-citrate, 0.06 ml 10× dispase/collagenase solution) for 10 min at 37°C.

Then, they were fixed in 4% *p*-formaldehyde for 30 min at room temperature. Brains were transferred to an ethanol-clean coverslip containing 16 µl PBS, covered with a slide and squashed (beaten with a needle onto the coverslip until disaggregation). Slides were immersed in liquid nitrogen, coverslips were removed and chromosomes were immunostained with αdH1K27me2 (1:200) or αdH1 (1:4000) as above. Images were recorded with a Leica SPE confocal microscope.

Salivary glands from *Drosophila w^{1118}* strain or from the indicated crosses (carried out at 29°C) were dissected from third instar larvae and polytene chromosomes prepared as described in (21). Primary antibodies used were: mouse αGFP (1:50), rabbit αGFP(1:400), rabbit αdH1 (1:4000), rat αHP1a (1:200), rabbit αdH1K27me2 (1:100), rabbit αH4K20me3 (1:100), and rabbit αH3K9me2 (1:100). Secondary antibodies (Jackson) were all used at 1:200. Images were recorded with a Leica SPE confocal microscope. For comparisons identical settings were used. From the same crosses immunostainings of whole salivary glands were performed on *p*-formaldehyde fixed salivary glands essentially as described (21) using αHP1a (1:200) and overnight incubation at 4°C. Images were taken in a Leica SPE confocal microscope and manually scored. When salivary glands were co-immunostained with rat αHP1a (1:200) and mouse monoclonal S9.6 (1:500) antibodies an initial wash in PBS, 0.5% SDS for 5 min followed by several washes in PBS, 0.3% Triton X-100 was included and incubation with the antibodies was left overnight at 4°C. Confocal images of whole glands mounts were recorded in a Leica SPE confocal microscope. For image analysis quantification, pixel integrated intensity of S9.6 immunostaining overlapping αHP1a immunostaining, which defined the chromocenter, was calculated and summed using FIJI software with an ad-hoc macro (kindly provided by Lídia Bardia, Advanced Digital Microscopy facility, IRB Barcelona).

RT-qPCR analysis

Total RNAs were extracted from 3rd instar larval imaginal disks and brains using RNAzol. Briefly, tissues from ∼50 larvae were homogenized in 400 µL of RNAzol, vortexed and then 100 µL of chloroform were added and vortexed again. The mix was left on ice for 3 min and spun in a microfuge for 5 min at max speed at 4°C. The upper phase was recovered and mixed with 70% ethanol (v/v) and the RNAs were purified using the RNeasy MinElute spin columns kit (Qiagen) according to manufacturer recommendations. Total RNA was nanodrop quantified and 1µg samples were reverse transcribed using the Transcriptor first cDNA strand kit (Roche) according to manufacturer indications and analyzed in triplicate for each biological sample by real-time qPCR analysis using specific primers (described in Supplementary Table SI) in a Quant Studio 5 Applied Biosystems apparatus.

Chromatin Immunoprecipitation (ChIP)

To a 25 mL-flask containing about 10^8 S2 cells, fresh formaldehyde was added until a final concentration of 1.8%

and incubated for 10 min at room temperature. Reaction was quenched by adding glycine up to 0.125 M and further incubating for 10 min at room temperature. Cells were harvested with a cell scraper and spun down. Cell pellets were resuspended in 5mL PBS and, subsequently, washed with 10 mL Lysis Buffer A (10 mM HEPES pH 7.9, 10 mM EDTA, 10 mM EGTA and 0.25% Triton X-100), spun and washed again with 10 mL Lysis Buffer B (10 mM HEPES pH 7.9, 100 mM NaCl, 1mM EDTA, 0.5 mM EGTA and 0.01% Triton X-100). A last washing step was done adding 4.5 mL TE and 0.5 mL SDS 10%. After spinning, pellets were resuspended in TE and PMSF was added up to 1 mM in a final volume of 4 mL where 40 µL of 10% SDS was added. Sonication was performed with BioRuptor by two sessions of 10 min with 30 s ON and 30 s OFF, on ice. Lysates were pooled in one tube, which was supplemented to obtain 1% Triton X-100, 0.1% Deoxycholate and 140 mM NaCl solution and incubated 10 min at 4°C. After spinning, supernatants containing chromatin were recovered to use them for the immunoprecipitation. To check DNA size, 100 µL of sonicated chromatin was de-crosslinked by adding SDS and NaHCO₃ to a final concentration of 1% and 0.1 M respectively, and incubating overnight at 65°C. Then, regular DNA extraction with phenol/chloroform was performed. Subsequently, DNA precipitation was done with 100% ethanol and 30 µL of 3 M sodium acetate followed by a washing step with 70% ethanol. Pellet was resuspended in 10 µL H_2O and incubated 30 min at 37°C with 0.5 µL RNAse A for RNA clearance. DNA sample was finally loaded on a 1.5% agarose gel to check DNA fragment size. Average size of DNA in these samples was ∼250 bp.

For chromatin immunoprecipitation, 500 µL aliquots of cross-linked chromatin were pre-cleared with 50 µL of Protein A Sepharose beads (PAS) resuspended in RIPA buffer at 50% (140 mM NaCl, 10 mM Tris–HCl pH 8, 1 mM EDTA, 1% Triton X-100, 0.1% SDS and 0.1% deoxycholate) and incubated for 1 h at 4°C. After centrifugation, supernatants were collected and incubated with 1 µL of αdH1K27me2 or 1 µL of αdH1 overnight at 4°C in a rotary wheel. Subsequently, 40 µL of PAS suspension were added to the samples and incubated for 3 h at 4°C. Washing steps with RIPA (×5), LiCl ChIP buffer (250 mM LiCl, 10 mM Tris–HCl pH 8, 1 mM EDTA, 0.5% NP-40 and 0.5% deoxycholate) (×1) and TE (×2) were performed (10 min each). Beads were incubated with 40 µL TE and 0.5 µL RNAse A (10 mg/mL) for RNA clearance (30 min, 37°C). Antibody-DNA conjugates were eluted by addition of 50 µL 0.2 M NaHCO₃ and 10 µL 10% SDS. After centrifugation, supernatants were collected. Beads were re-extracted twice with 100 µL of Elution Buffer (1% SDS and 0.1M NaHCO₃) and supernatants pooled (300 µL). A sample input of 50 µL of cross-linked chromatin was resuspended in Elution Buffer to obtain a final volume 300 µL. Both IP samples and Inputs were incubated overnight at 65°C. Then 3 µL of Proteinase K (at 10 mg/ml) were added and samples were incubated 3 h at 56°C. DNA was phenol/chloroform extracted and ethanol precipitated overnight at −20°C. Finally, DNA pellets were resuspended in 15 µL H_2O. DNA concentrations were determined by Qbit fluorometric quantitation. For ChIPseq experiments samples were then sent to

an external facility for high-throughput Illumina sequencing. For ChIP-qPCR experiments, real-time qPCR analysis from samples prepared as described above was performed in triplicate using the Light Cycler system (Roche) and a Light Cycler 480 apparatus as described in (22). Primers used in these experiments are described in Supplementary Table SI.

ChIPseq analysis

Analysis of ChIPseq data was performed essentially as described (18). Quality of original FASTQ sequences were assessed using FASTQC v0.11. FASTQ files were aligned against the dm3 genome assembly using Bowtie (v2.2.2) using options -n 1 and replicates were pooled into a single BAM file. Potential overamplification artifacts were detected and removed using sambamba v0.5.1. IP versus input enrichment assessment was performed using the htSeqTools R package version 1.12.0. and TDF coverage tracks were generated using IGVTools 2. Peak calling between duplicate filtered IP and Input samples was performed using MACS 1.4.2, using options -g dm and the resulting peaks were annotated against the dm3 genome using ChIPPeakAnno 3.16.1. Asessment of the presence of repeat and repetitive elements among called peaks was determined using Repeat-Masker v4.3.0, with options -no-is and -species drosophila.

For dH1K27me2 ChIPseq, identified peak sequences were scanned for known and *de-novo* motifs using Homer version 2. A cluster analysis of read similarity was performed with those reads that failed to align in both ChIP samples and Input, by means of the CD-Hit software (v 4.5.4) (18). First, reads were grouped into a single Fasta file and flagged with their corresponding tag (ChIP or Input). Then, reads were sorted decreasingly by length and a sequence clustering was performed using a greedy incremental algorithm. The longest read became the representative of the first cluster and the remaining reads were compared to the representatives of existing clusters. If the similarity with any representative was above the given thresholds, it was grouped into that cluster. Otherwise, a new cluster was defined with that read as the representative. The thresholds used were sequence identity and alignment coverage. The sequence identity threshold used was the number of identical nucleotides in the alignment divided by the full length of the shorter sequence which should be equal or bigger than 0.95. Secondly, the alignment should cover a 40% of the length of both sequences. Then, the proportion of reads between ChIP samples and Input for each cluster was tested with a hypergeometric test with a Benjamini-Yekuteli adjusted *P*-value <0.01.

ChIPseq data are deposited at NCBI GEO (GSE167018, GSE127227).

RESULTS

dH1K27me2 is detected throughout development and across cell types

To analyze dH1K27me2 content across fly development we performed WB and IF analyses using αdH1K27me2 antibodies. Specificity of the αdH1K27me2 antibodies used in these experiments was shown in transgenic flies carrying UAS-constructs expressing either a wild-type dH1::GFP fused protein or a mutated dH1K27A::GFP form, which carries a K27A mutation that prevents methylation. Both constructs were expressed in salivary glands using the UAS/GAL4 system. Briefly, transgenic flies carrying dH1::GFP or dH1K27A::GFP constructs under the control of a minimal UAS promoter, which bears binding sites for the yeast transcription factor GAL4, were crossed with transgenic driver flies expressing the yeast transcription factor GAL4 under the control of an appropriate fly promoter to induce expression of the transgenic UAS-construct in salivary glands (*i.e. Da*-GAL4*, Nub*-GAL4, *Act*-GAL4). WB analysis of salivary glands extracts showed that both constructs were expressed to similar levels as detected using αGFP (Supplementary Figure S1A, right panel). However, while αdH1K27me2 antibodies detected dH1::GFP in WB, they failed to detect the mutated dH1K27A::GFP protein (Supplementary Figure S1A, left panel). In addition, previous *in vitro* dot-blot assays using dH1 peptides containing K27me2, K28me2 or unmethylated K27 showed high selectivity of αdH1K27me2 for the methylated dH1K27me2 peptide (13) (see also Supplementary Figure S1B, left). Furthermore, αdH1K27me2 showed no significant reactivity against an H3 peptide carrying K9me3 (Supplementary Figure S1B, right panel). During embryo development, dH1 expression is zygotic being first detected around 2h after egg laying concomitant with the activation of the zygotic genome (ZGA) (11). We observed that dH1K27me2 appears as early as dH1 expression is detected (Figure 1A, lanes 1–4). Later, dH1K27me2 was also detected in third instar larvae in brains, imaginal disks and salivary glands, as well as in head and abdomen of adult male and female flies (Figure 1B).

In good agreement with these results, IF experiments performed in brain squashes of third instar larvae detected intense nuclear αdH1K27me2 immunostaining in interphase cells (Figure 1C). Similarly, in cultured S2 cells, a roughly uniform nuclear αdH1K27me2 immunostaining was observed in interphase (Figure 1D). Interestingly, αdH1K27me2 signal was generally detected at HP1a foci that mark pericentromeric heterochromatin (Figure 1D), where it highly concentrated in some cells (Figure 1D). Intense αdH1K27me2 immunostaining was also detected in the specialized interphase polytene chromosomes of salivary glands (Figure 2A). Notably, dH1K27me2 largely colocalized with HP1a at the chromocenter (Figure 2A and B), which corresponds to the fused pericentromeric heterochromatin regions of all four *Drosophila* chromosomes. αdH1K27me2 immunostaining was also observed all along the chromosome arms (Figure 2A). Overall dH1K27me2 distribution in the arms matched nicely with DAPI intense bands (Figure 2A and C), which have high dH1 content (23–25) and correspond to intercalary heterochromatic regions enriched in transposable elements and other repetitive DNA sequences (26,27). Noteworthy, while an intense HP1a immunostaining was observed on the heterochromatic chromosome 4, dH1K27me2 presence on chromosome 4 was low and mostly restricted to two weak bands that colocalized with DAPI bands (Figure 2B). Remarkably, dH1K27me2 was not detected at other HP1a positive regions outside the chromocenter, namely euchromatic and telomeric regions (Supplementary Figures S2A and B).
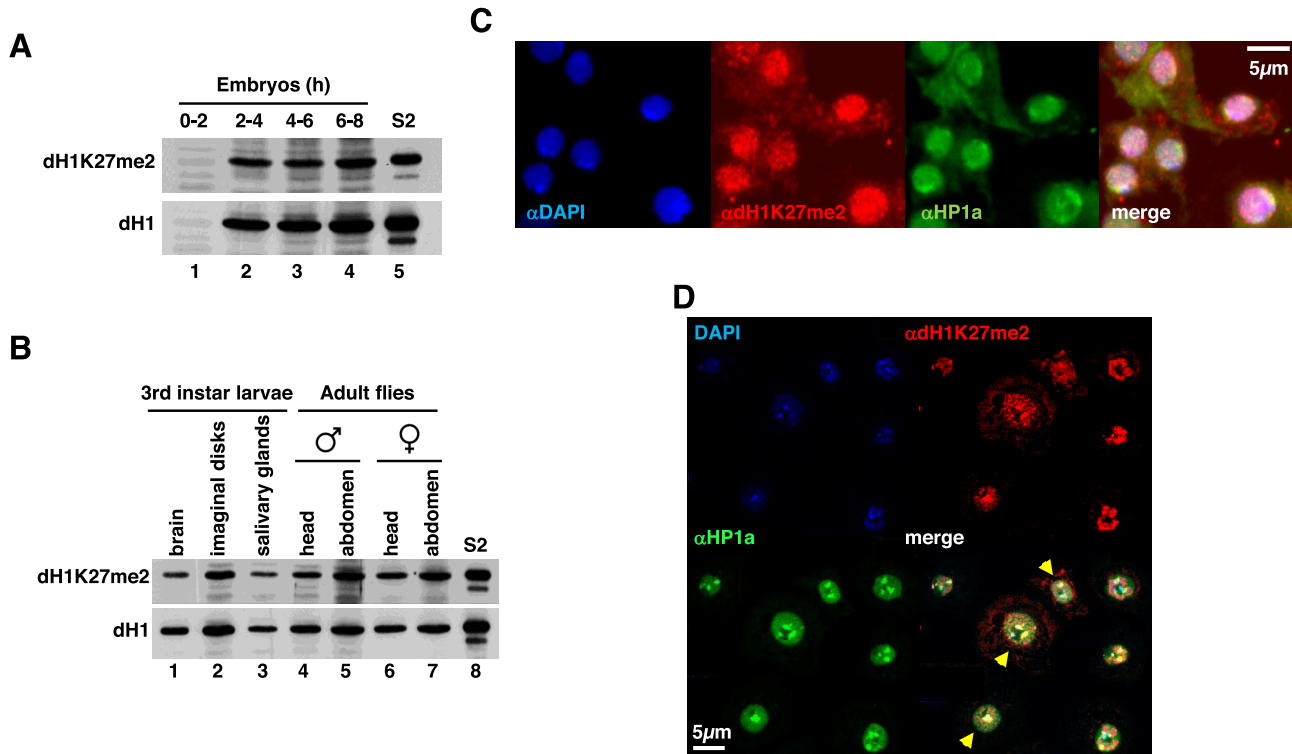
Figure 1. Ubiquitous expression of dH1meK27me2. (**A**) WB analysis with αdH1 and αdH1K27me2 of perchloric acid (PCA) extracts from w^{1118} embryos staged after egg laying for the indicated time periods (lanes 1–4). Lane 5 shows a PCA extract from S2 cells as control. (**B**) WB analysis with αdH1 and αdH1meK27me2 of PCA extracts from the indicated w^{1118} larval organs (lanes 1–3), and head and abdomen of adult male (lanes 4 and 5) and female (lanes 6 and 7) flies. Lane 8 shows a PCA extract from S2 cells as control. (**C**) Immunostaining of w^{1118} larval brain squashes with αdH1K27me2 (in red) and αHP1a (in green). DNA was stained with DAPI (in blue). Scale bar corresponds to 5 μm. (**D**) Immunostaining of interphase S2 cells with αdH1K27me2 (in red) and αHP1a (in green). DNA was stained with DAPI (in blue). Yellow arrows indicate nuclei in which αdH1K27me2 signal accumulates at αHP1a foci. Scale bar corresponds to 5μm.

dH1K27me2 accumulates in heterochromatin

Previous results (13) showed that, in S2 cells, αdH1K27me2 immunostaining was largely restricted to pericentromeric heterochromatin in metaphase chromosomes. Here, we further confirmed this observation (Figure 3B, top panel) and extended it to metaphase chromosomes of larval neuroblasts (Figure 3A, left panel) and of a second cell line (Kc167) (Figure 3C). Note that immunostaining with αdH1 antibodies, which recognize total dH1, showed no such restriction at pericentromeric heterochromatin (Figure 3A, right panel, and B, bottom panel). To gain further insights on the genomic distribution of dH1K27me2, we performed ChIPseq analysis in S2 cells. This analysis identified 4,751 dH1K27me2 enriched regions (Supplementary Table SII). Most of these regions clustered proximal to the pericentromeric heterochromatic regions of chromosomes 2 and 3, in the assembled heterochromatic regions of chromosomes 2 and 3 (chr2L&RHet and chr3L&RHet) and at the unassembled repetitive heterochromatic elements of the artificial chromosomes U and Uextra (Figure 4A). dH1K27me2 enriched regions usually appeared in clusters and extended for several kilobases (up to ∼70 kb) that, in some cases, could be interrupted by gene-containing regions of low dH1K27me2 content (Supplementary Figure S3, top panel). Silenced heterochromatic gene clusters, such as the *stellate* locus in pericentromeric heterochromatin of chro-

mosome X, were also found enriched in dH1K27me2 (Supplementary Figure S3, bottom panel). Interestingly, only 4 dH1K27me2 enriched regions were detected on the heterochromatic chromosome 4, in good agreement with IF results reported above (Figure 2B). Moreover, although only 38% ($N = 1805$) of the dH1K27me2 enriched regions could be assigned to any particular chromatin state according to the *Drosophila* 9 chromatin states model (3), the vast majority of those (90%, $N = 1603$) overlapped with heterochromatin state 7 (Figure 4B), which is characterized by high levels of H3K9me2/me3, HP1a and Su(var)3–9 (3). This enrichment was statistically significant as shown by permutation analysis (Figure 4C), while no significant overlap was observed with any of the other chromatin states even after removing all reads overlapping chromatin state 7. The high proportion of non-assigned (NA) dH1K27me2 enriched regions reflects their high abundance at the unassembled artificial heterochromatic chromosomes U and Uextra, which are not included in the *Drosophila* 9 chromatin states model (3). A large majority of the dH1K27me2 enriched regions (4683 regions, >98%) mapped to repetitive DNA sequences (Figure 4D). These included many transposable elements (TEs), both LTR and non-LTR retrotransposon and DNA transposons, but also long repeat sequences, satellite DNAs and a long list of simple repeated DNA sequences (Supplementary Tables SIII and SIV). In good agreement
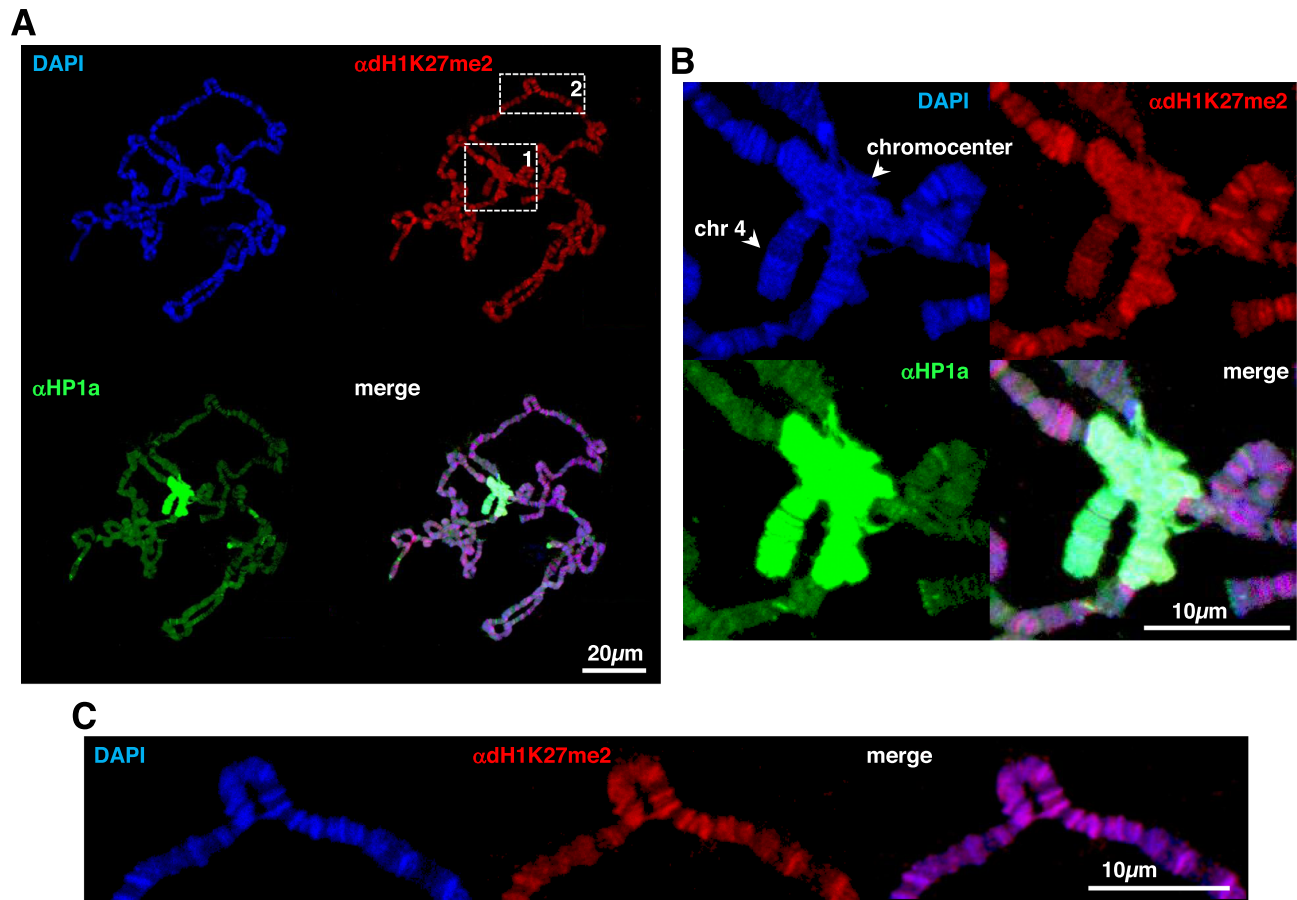
Figure 2. dH1K27me2 pattern in polytene chromosomes. (**A**) Immunostaining of w^{1118} polytene chromosomes with αdH1K27me2 (in red) and αHP1a (in green). DNA was stained with DAPI (in blue). Scale bar corresponds to 20μm. (**B**) Enlarged image of region 1 in A. Arrows indicate the chromocenter and chromosome 4. Scale bar corresponds to 10 μm (**C**) Enlarged image of region 2 in A showing overlapping of αdH1K27me2 bands (in red) with DAPI bands (in blue). Scale bar corresponds to 10 μm

with these results, ChIP-qPCR experiments detected significant dH1K27me2 enrichment in ten selected TEs with respect to a negative control region (Figure 4E). Enrichments ranged from 3-fold to 20-fold depending on the element analyzed. These regions were also enriched in H3K9me2 and H4K20me3, reflecting their heterochromatic character (Figure 4E). We also observed that an unusually high proportion of the reads (21–45%, depending on the replicate) failed to align to the reference genome. A cluster analysis of sequence similarity performed with the unaligned reads showed that they were highly enriched in uncatalogued simple repeat sequences (Supplementary Table SV).

ChIPseq experiments with αdH1 antibodies, which recognize total dH1, confirmed the specific accumulation of dH1K27me2 at heterochromatic regions. dH1 is known to be enriched at heterochromatic regions, but its genomic distribution is not constrained to heterochromatin being detected all across the genome (25,28). Consequently, as expected, we observed that αdH1K27me2 and αdH1 ChIP signals were both high at heterochromatic regions, showing similar profiles (Figure 4F, top panel). However, in euchromatic regions, αdH1 ChIP signal was much higher than αdH1K27me2 ChIP signal (Figure 4F, bottom panel). In fact, the fraction of total ChIPseq reads de-

tected at dH1K27me2 enriched regions was much higher in αdH1K27me2 than in αdH1 ChIPseq data (Figure 4G), confirming the specific accumulation of dH1K27me2 in heterochromatin.

Altogether these results strongly suggest that dH1K27me2 is largely constrained to heterochromatic regions. Interestingly, DNA sequence motif analysis of the dH1K27me2 regions showed statistically significant enrichment in several motifs that, contrary to our expectations, were complex, did not represent any known satellite DNA sequences or simple repeats, and scored as binding sites for several transcription factors (TFs) (Supplementary Table SVI).

dH1K27me2 contributes to heterochromatin organization independently of H3K9 methylation

Next, we addressed the contribution of dH1K27me2 to heterochromatin organization. For this purpose, we analyzed the effects of expressing wild-type dH1::GFP and mutant dH1K27A::GFP using the UAS/GAL4 system (see above). For these experiments we used *Da*-GAL4, *Nub*-GAL4 and *Act*-GAL4 drivers and analyzed the effects in polytene chromosomes from salivary glands. WB analy-
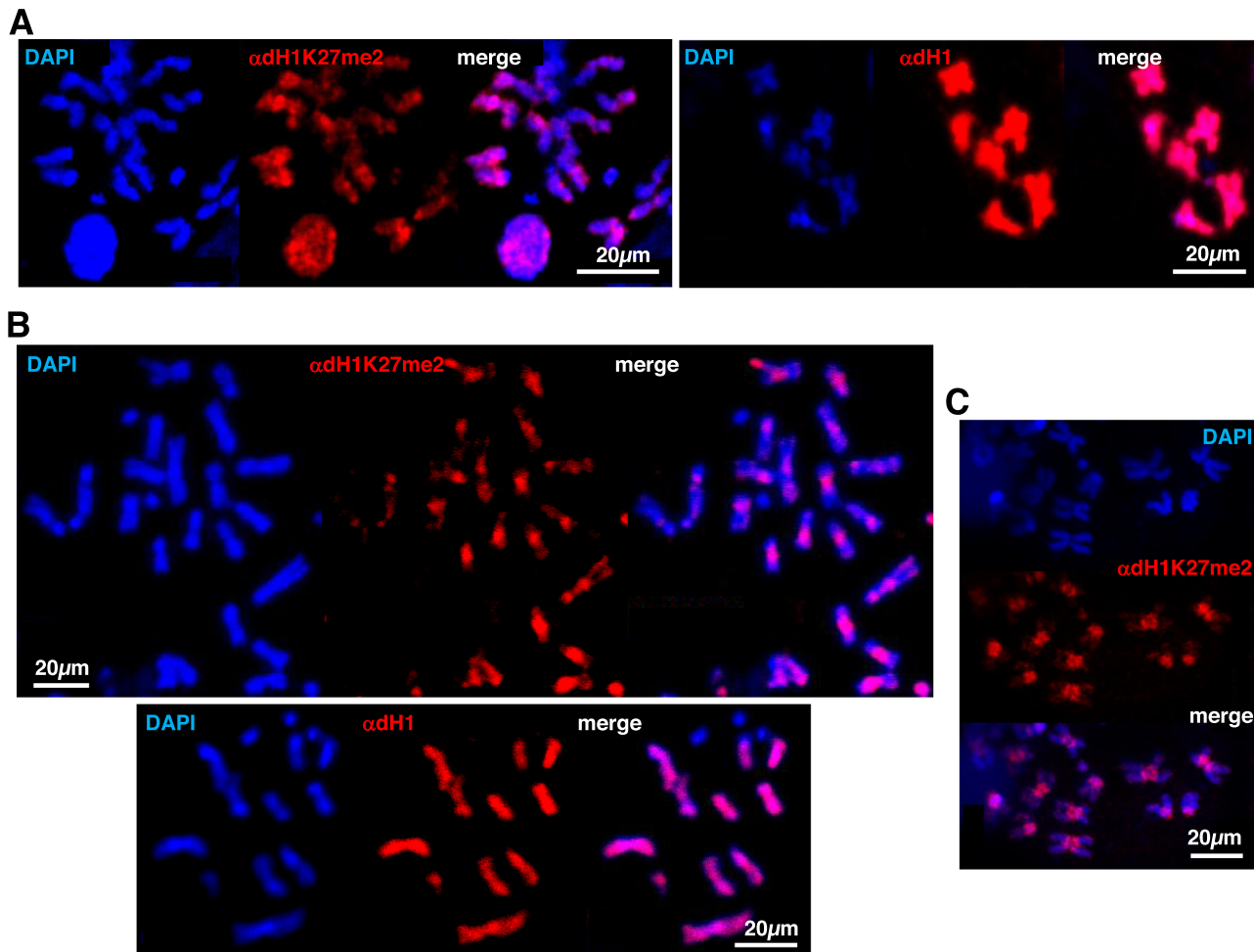
Figure 3. Pericentromeric accumulation of dH1K27me2 in metaphase chromosomes. (**A**) Metaphase chromosome spreads from w^{1118} larval brain squashes immunostained with αdH1K27me2 (in red, left) and αdH1 (in red, right). DNA was stained with DAPI (in blue). Scale bars correspond to 20μm. (**B**) Metaphase chromosome spreads from S2 cells immunostained with αdH1K27me2 (in red, top) and αdH1 (in red, bottom). DNA was stained with DAPI (in blue). Scale bars correspond to 20 μm. (**C**) Metaphase chromosome spreads from Kc167 cells immunostained with αdH1K27me2 (in red). DNA was stained with DAPI (in blue). Scale bar corresponds to 20 μm.

sis of total salivary glands extracts showed that, independently of the driver used, both constructs were expressed to similar levels, without detectably affecting the levels of endogenous dH1 (Supplementary Figure S4A). In addition, IFs experiments showed that both constructs had similar patterns of localization in polytene chromosomes (Supplementary Figure S4B). However, we observed that, in comparison to control polytene chromosomes (Figure 5A, top panel), expression of mutant dH1K27A::GFP strongly reduced αdH1K27me2 immunostaining both at the chromocenter and along the chromosome arms (Figure 5A, bottom panel), while no such reduction was observed upon overexpression of wild-type dH1::GFP (Figure 5A, center panel). In these experiments, salivary glands from flies expressing dH1K27A::GFP or dH1::GFP were squashed and immunostained together with salivary glands from control flies. In this way, variability due to immunostaining conditions was minimized, while control and expressing polytene chromosomes were easily distinguished on the basis of their GFP content. These results suggest that expression of

dH1K27A competes endogenous dH1 and, consequently, reduces dH1K27me2 levels.

Notably, IF experiments in whole salivary glands showed that, concomitant to reduced dH1K27me2, expression of dH1K27A::GFP caused a > 2-fold increase in the frequency of cells showing a split chromocenter, in comparison to expression of wild-type dH1::GFP (Figure 6A). In addition, we observed that expression of dH1K27A::GFP significantly upregulated expression of several heterochromatic TEs elements, as shown by RT-qPCR (Figure 6B). Furthermore, IF experiments using S9.6 antibodies, which recognize RNA:DNA hybrids (R-loops), detected a significant increase in S9.6 signal overlapping with αHP1a signal at the heterochromatic chromocenter of salivary gland nuclei expressing dH1K27A::GFP, in comparison to those expressing dH1::GFP (Figure 6C). Altogether these results indicate that expression of mutant dH1K27A::GFP impacts heterochromatin organization, impairing silencing of heterochromatic TEs and enhancing R-loops formation in heterochromatin.
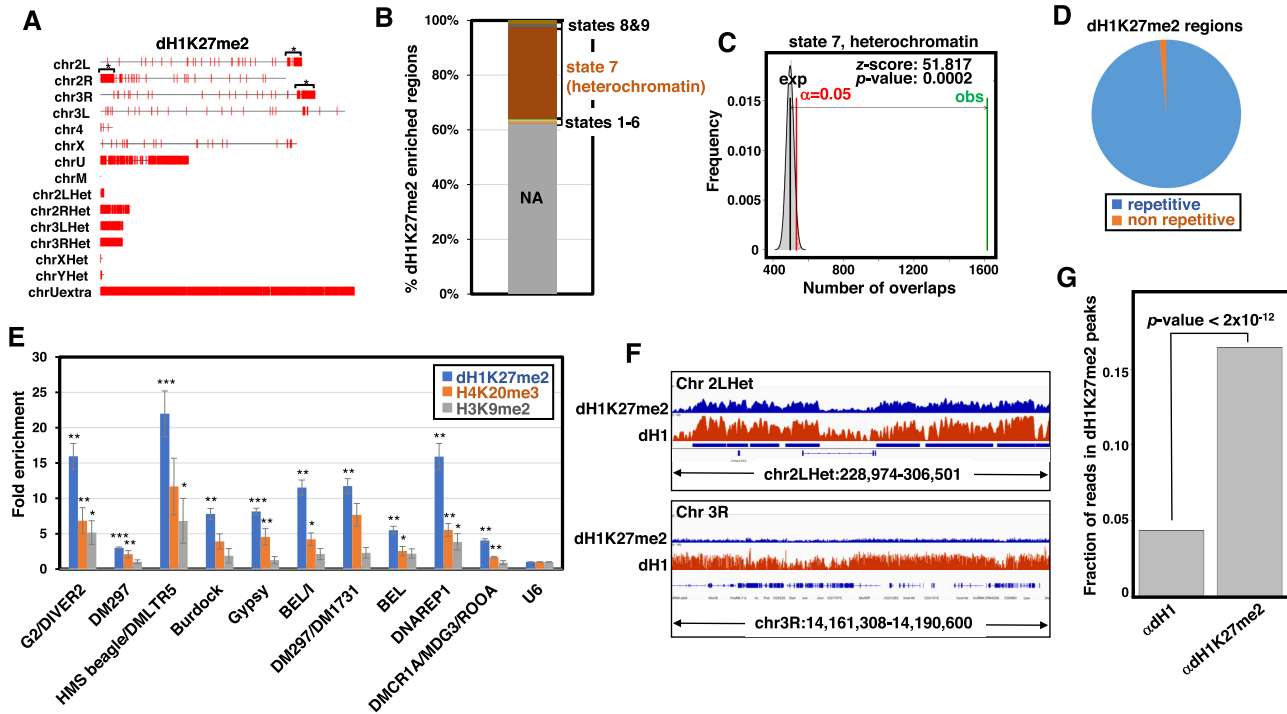
Figure 4. αdH1K27me2 ChIPseq analysis in S2 cells. (**A**) Chromosomal distribution of the identified dH1K27me2 enriched regions. chr2L and chr2R, and chr3L and chr3R correspond to chromosome 2 and 3 left and right arms respect to the position of the centromere, respectively. Asterisks indicate dH1K27me2 enriched regions clustering at pericentromeric regions. chr4 and chrX are oriented with the centromere to the right. chr2LHet, chr2RHet, chr3LHet, chr3RHet, chrXHet and chrYHet correspond to partially assembled pericentromeric heterochromatin regions of the indicated chromosomes. chrU and chrUextra correspond to unassembled highly repetitive heterochromatic regions. chrM corresponds to the mitochondrial chromosome. (**B**) The proportion of dH1K27me2 enriched regions assigned to each of the nine chromatin epigenetic states according to (3). NA: dH1K27me2 enriched regions that could not be assigned to any chromatin state. (**C**) Permutation analysis showing statistical significance of the association of dH1K27me2 enriched regions with chromatin state 7 (heterochromatin) according to (3). The frequency of the number of overlaps is presented based on 5000 random permutations of the experimentally identified regions. The average expected number of overlaps (black) is compared with the observed number of overlaps (green). The $\alpha = 0.05$ confidence interval is indicated (red). z-score and permutation test *P*-value of the difference are also indicated. (**D**) Pie graph showing the proportion of identified dH1K27me2 enriched regions as a function of their content in repeated sequences. (**E**) ChIP-qPCR analysis with αdH1K27me2 (blue bars), αH4K20me3 (red bars) and αH3K9me2 (gray bars) at the indicated genomic region is presented as the fold enrichment respect to *U6* as a control region. Error bars are s.e.m. *P*-values respect to *U6* are indicated (*<0.1; **<0.05; ***<0.001; two-tailed Student's *t*-test). (**F**) Coverage profiles for αdH1 and αdH1K27me2 ChIPseqs are presented for the indicated genomic regions. Genomic organization and Dm3 coordinates of the regions are indicated. Blue bars indicate dH1K27me2-enriched regions. (**G**) The fraction of total ChIPseq reads at dH1K27me2 enriched regions are presented for αdH1 and αdH1K27me2 ChIPseqs (*P*-value $< 2.2 \times 10^{-16}$; Pearson's chi-squared test with Yates' continuity correction).

Next, we analyzed whether dH1K27A::GFP expression affects H3K9 methylation and HP1a binding, which are hallmarks of heterochromatin formation (5). IF experiments in polytene chromosomes showed that dH1K27A::GFP expression did not affect H3K9me2 and HP1a levels at the chromocenter (Figure 7A). In agreement, WB analysis showed that total levels of both HP1a and H3K9me2 were not detectably affected in salivary glands (Figure 7B). These results suggest that the contribution of dH1K27me2 to heterochromatin organization is largely independent of H3K9 methylation and HP1a binding. To further analyze the relationship between dH1K27me2 and H3K9 methylation, we performed IF experiments in polytene chromosomes from flies carrying a H3K9R mutation that prevents H3K9 methylation. In these flies, deletion of the complete *HisC* locus, which contains ~100 tandemly repeated copies of the 5kb histone repeat that carries one copy of each histone gene, was complemented by a transgenic construct containing 12 copies of the histone

monomer either wild type (12× WT) or carrying a H3K9R mutation (12× H3K9R) (15). We observed that in H3K9R mutant flies the levels of H3K9me2 at the chromocenter were markedly reduced in polytene chromosomes (Figure 8A). In agreement, HP1a localization at the chromocenter was heavily reduced (Figure 8A and B) (15). Remarkably, the pattern of dH1K27me2 remained largely unaffected since no signs of reduction at the chromocenter or redistribution could be appreciated (Figure 8B). Along the same lines, depletion of Su(var)3–9, which is responsible for H3K9 methylation at the chromocenter (29), did not affect the pattern of dH1K27me2. In these experiments, to minimize variability due to immunostaining conditions, salivary glands from knockdown *Su(var)3–9^{RNAi}* flies were squashed and immunostained together with salivary glands from control flies expressing an H2AvD2::GFP fusion protein. We observed that Su(var)3–9 depletion, which strongly reduced H3K9me2 (Supplementary Figure S5A), did not affect the overall pattern of dH1K27me2, nor its
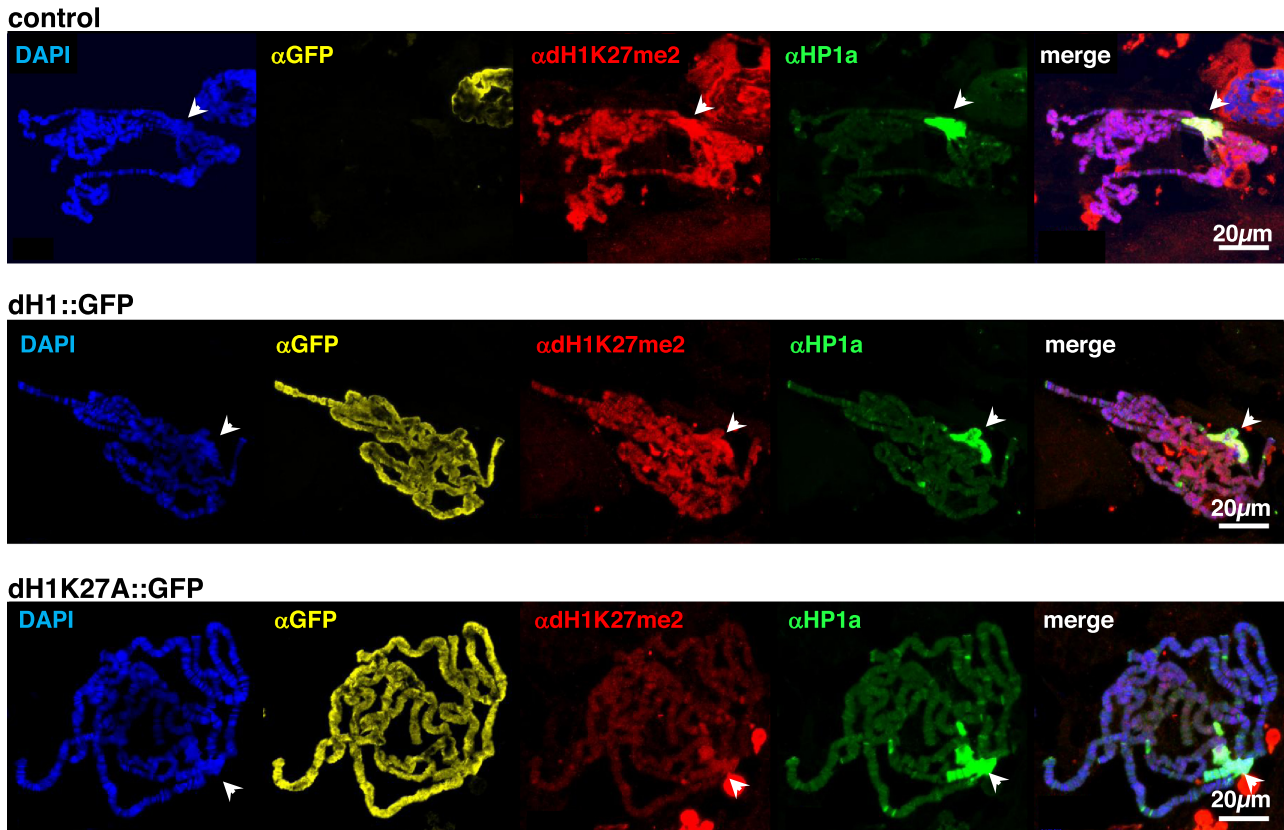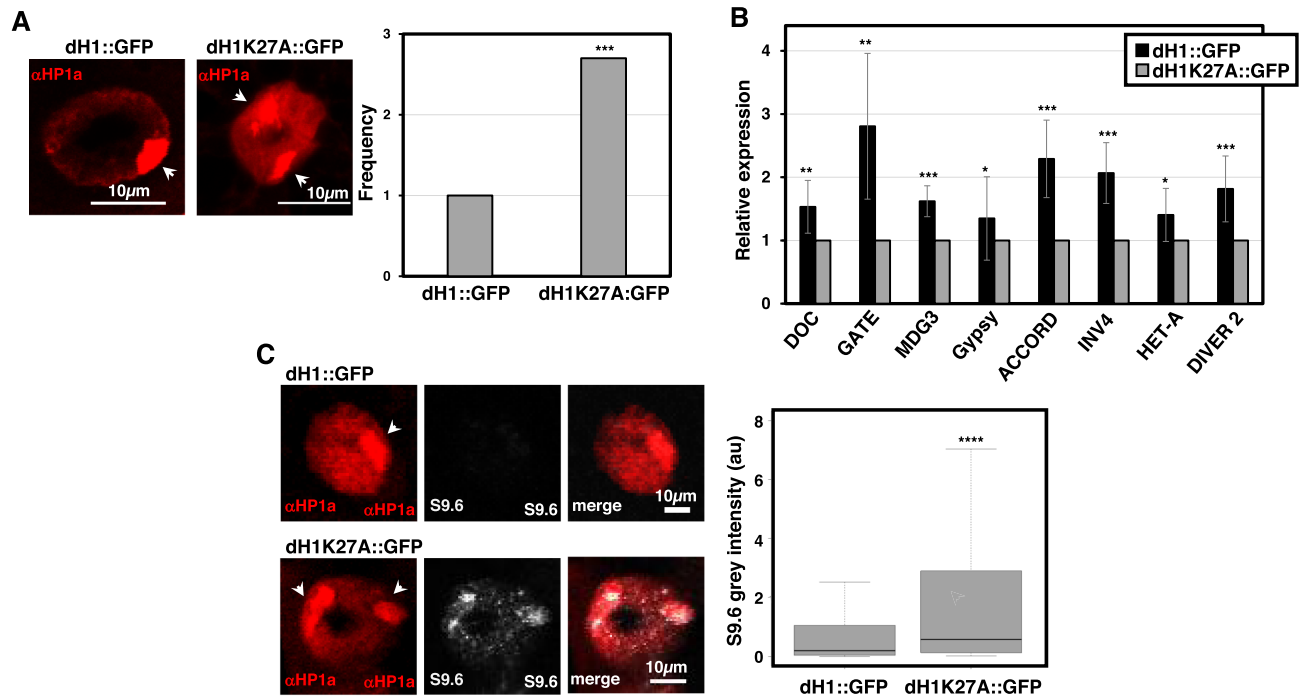
Figure 5. Expression of dH1K27A::GFP reduces dH1K27me2. Polytene chromosomes from flies expressing wild-type dH1::GFP (center) and mutant dH1K27A::GFP (bottom) were mixed with polytene chromosomes from control flies (top) and co-immunostained with αGFP (in yellow, to distinguish control and GFP-expressing chromosomes), αdH1K27me2 (in red) and αHP1a (in green). Expression was induced with *Nub*-GAL4 at 29°C. DNA was stained with DAPI (in blue). Arrowheads indicate the chromocenter. Scale bars correspond to 20 μm.

accumulation at the chromocenter (Supplementary Figure S5B). Similar experiments showed that HP1a depletion had no effect either on the pattern of dH1K27me2 (Supplementary Figure S6). Another important hallmark of heterochromatin is H4K20 trimethylation by Su(var)4–20, which is recruited to heterochromatin by HP1a and H3K9 methylation (6,7). We observed that the pattern of dH1K27me2 distribution in polytene chromosomes was not affected either by depletion of Su(var)4–20 (Supplementary Figure S7B), while H4K20me3 was strongly reduced (Supplementary Figure S7A). Altogether these results indicate that dH1K27me2 at heterochromatin is independent of the main H3K9 methylation pathway of heterochromatin formation.

Next, in an effort to identify the enzymes involved in dH1K27 methylation/demethylation, we performed a candidate screen of several known histone lysine methyltransferases (HMTs) and demethylases (KMDs). For this purpose, we performed IF experiments in polytene chromosomes with several RNAi-mediated knockdown and overexpression conditions. In these experiments, in addition to Su(var)3–9 (Supplementary Figure S5) and Su(var)4–20 (Supplementary Figure S6), we tested the HMTs SETDB1(egg), G9a and E(z), and the KDMs 4A, 4B and 5(Lid). Regretfully, all these assays gave negative results (data not shown).

DISCUSSION

The contribution of linker histones H1 to the epigenetic regulation of chromatin functions is currently under active investigation since increasing evidence is pointing out to far more than its known structural role (1). In this regard, like core histones, linker histones H1 are subjected to multiple PTMs, which are anticipated to have important contributions to the regulation of their functions. However, to date, data on their genomic distribution and functional contribution are scarce. Here we have provided strong evidence for dH1K27me2 as a new epigenetic modification that contributes to heterochromatin organization in *Drosophila*. dH1K27me2 is detected as early as histone H1 is expressed at cellularization and heterochromatinization begins (30), and, thereafter, throughout development. Our results suggest that dH1K27me2 associates with heterochromatin throughout the cell cycle. In mitosis, dH1K27me2 strongly accumulates at pericentromeric heterochromatin. However, in interphase, dH1K27me2 shows a broader genomic distribution. In the interphase polytene chromosomes, dH1K27me2 is detected in pericentromeric heterochromatin at the chromocenter, but, also, in intercalary heterochromatin at DAPI-intense bands. Similarly, in interphase cells, dH1K27me2 is not constrained to pericentromeric heterochromatin since significant αdH1K27me2 reactivity is detected at regions that do not show detectable

Figure 6. Expression of dH1K27A::GFP impacts heterochromatin organization. (**A**) Expression of dH1K27A::GFP results in a split-chromocenter phenotype. On the left, nuclei in whole salivary glands from flies expressing dH1::GFP (left) and dH1K27A::GFP (right) were immunostained with αHP1a (in red). Expression was induced with *Da*-GAL4. Arrowheads indicate the chromocenter. Scale bars correspond to 10 μm. On the right, quantitative analysis of the results. The normalized frequencies of nuclei showing split chromocenter are shown for flies expressing dH1::GFP ($N = 280$) or mutant dH1K27A::GFP ($N = 325$). (*P*-value: ***<0.001; two-tailed Fischer F exact test). (**B**). RT-qPCR analysis of total RNAs extracted from larvae overexpressing dH1::GFP or dH1K27A::GFP. Expression was induced with *Da*-GAL4. Results were normalized to RPL32 and fold changes vs dH1::GFP are presented. Error bars are s.e.m. *P*-values are indicated (**$P < 0.05$, ***$P < 0.01$; Benjamini–Hochberg mixed linear model). (**C**) Expression of dH1K27A::GFP enhances R-loops formation at the chromocenter. On the left, immunostaining with S9.6 antibodies (in gray) and αHP1a (in red) of nuclei from intact salivary glands expressing dH1::GFP or dH1K27A::GFP. Expression was induced with *Da*-GAL4. Arrowheads indicate the chromocenter. Scale bar corresponds to 10 μm. On the right, quantitative analysis of the results. The integrated grey intensity with S9.6 at the chromocenter is shown for nuclei from intact salivary glands expressing dH1::GFP ($N = 699$) or dH1K27A::GFP ($N = 405$). (*P*-value: ****< 0.0001; Kruskal–Wallis test).

αHP1a immunostaining. ChIPseq analysis suggests that these regions correspond to intercalary heterochromatin since the vast majority (>98%) of dH1K27me2 enriched sites detected in asynchronous S2 cell cultures, in which the proportion of mitotic cells is <5%, maps to repeated DNA elements, both TE and simple repeat sequences. These observations suggest that dH1K27me2 genomic distribution during cell cycle progression is dynamic, being removed from intercalary heterochromatin in mitosis to accumulate at pericentromeric heterochromatin.

Interestingly, dH1K27me2 was not found enriched in chromosome 4, despite it is heterochromatic and enriched in both H3K9me2 and HP1a. Of note, the mechanisms behind heterochromatin formation in chromosome 4 are different since H3K9 methylation and HP1a binding depend on SETDB1 instead of Su(var)3–9 as in pericentromeric heterochromatin (31–33). Along the same lines, dH1K27me2 was not detected at telomeres, which are also heterochromatic and enriched in HP1a. In this regard, our ChIPseq analysis detected dH1K27me2 enrichment at the telomeric HET-A and TART retrotransposons. However, this enrichment likely reflects the presence of dH1K27me2 at pericentromeric heterochromatin of chromosomes Y and III, where HET-A and TART are also present (27,34,35). Finally, HP1a is detected at several euchromatic

regions where, paradoxically, it is required for gene expression (36). At these regions, dH1K27me2 was neither detected.

Altogether these results indicate that dH1K27me2 is largely restricted to pericentromeric and intercalary heterochromatic regions, but it is absent from other types of heterochromatic regions. Consistent with its preferential localization in heterochromatin, the presence of dH1K27me2 strongly correlates with other heterochromatic marks, namely H3K9me2 and, specially, H4K20me3. Interestingly, while H3K9me2 is mostly constrained to the chromocenter and chromosome 4, the pattern of H4K20me3 distribution in polytene chromosomes strongly resembles that of dH1K27me2, being detected at the chromocenter and in the DAPI-intense bands of intercalary heterochromatin, but largely absent from chromosome 4 (7). In addition, H4K20me3 distribution in human metaphase chromosomes is strikingly similar to the dH1K27me2 distribution observed here in fly cells (37). Finally, H4K20me3 localization in C127 cells has also been suggested to be cell cycle regulated (7).

Histones H1 have been reported to be more mobile than core histones (38,39), opening the question of how any given H1 PTM can be restricted to a specific chromatin region, such as dH1K27me2 in heterochromatin. Currently, mecha-
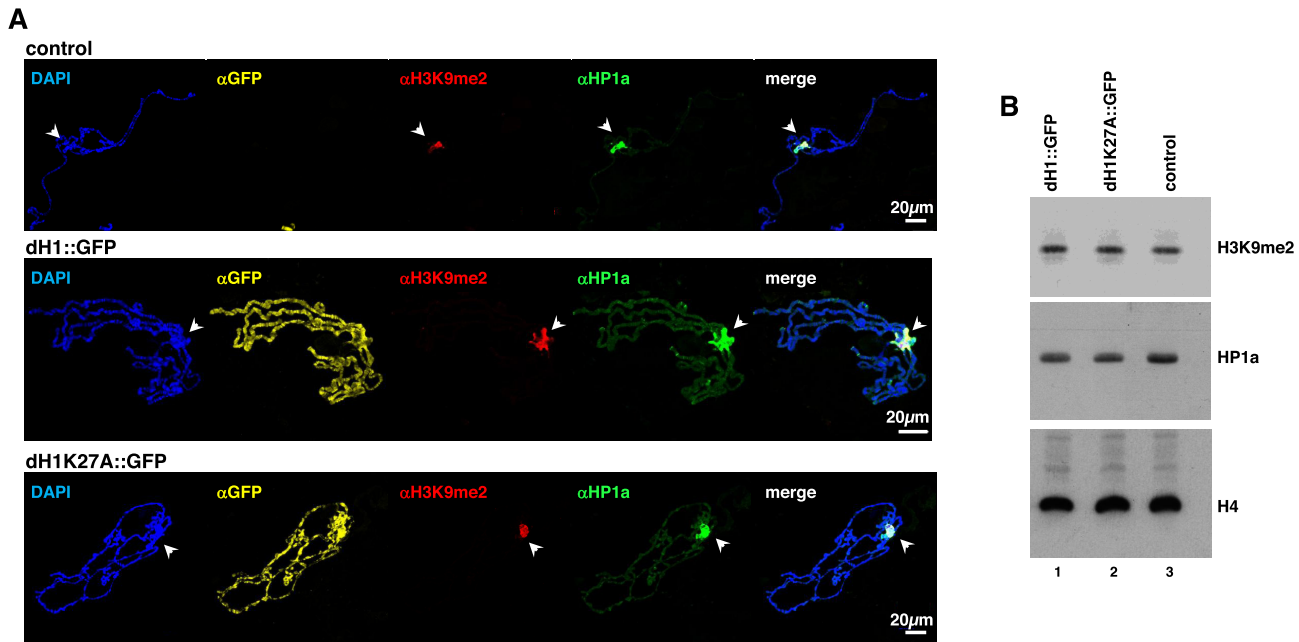
Figure 7. dH1K27A expression does not affect H3K9 methylation and HP1a binding. (**A**) Polytene chromosomes from flies expressing dH1::GFP (center) and mutant dH1K27A::GFP (bottom) were mixed with polytene chromosomes from control flies (top) and co-immunostained with αGFP (in yellow, to distinguish control and GFP-expressing chromosomes), αH3K9me2 (in red) and αHP1a (in green). Expression was induced with *Nub*-GAL4. DNA was stained with DAPI (in blue). Arrowheads indicate the chromocenter. Scale bars correspond to 20 μm. (**B**) WB analysis with αH3K9me2 (upper), αHP1a (center) and αH4 (bottom) of total salivary glands extracts obtained from control flies and flies expressing dH1::GFP and mutant dH1K27A::GFP.

nisms that could restrict H1's mobility are largely unknown. However, in this regard, it has been shown that, in mammals, H1s exist as two fractions of different mobility, the less mobile of which is enriched in heterochromatin (38).

dH1 is known to have a crucial contribution to heterochromatin organization and stability (17,25,40,41). Our results suggest that, at least to some extent, this contribution involves dH1K27me2 since expression of a mutated dH1K27A construct, which impairs dH1K27me2, induces a split-chromocenter phenotype, upregulates expression of heterochromatic transposons and induces R-loops accumulation in heterochromatin. Similar phenotypes were previously reported upon dH1 depletion (17,25,40,41), suggesting that, regarding heterochromatin organization and function, impairing dH1K27me2 mimics dH1 loss-of-function. Notably, reduced dH1K27me2 observed upon dH1K27A expression does not affect H3K9 methylation and, *vice versa,* impairing H3K9 methylation does not alter dH1K27me2, suggesting that dH1K27 methylation and H3K9 methylation act largely independently in heterochromatin formation. It has been proposed that dH1 directly interacts with Su(var)3–9 and is responsible for its tethering to pericentromeric heterochromatin, enhancing its H3K9 methylation activity (25,40). Our results cannot exclude the possibility that, besides a direct contribution of dH1K27me2, dH1 also contributes to heterochromatin formation by recruiting Su(var)3–9 in a dH1K27me2-independent manner. Intriguingly, it has been reported that, although H3K9me2 becomes undetectable in polytene chromosomes upon dH1 depletion, total H3K9me2 levels actually increase (25), suggesting that dH1 depletion might not affect H3K9 methylation *per se*, but, instead, it might destabilize H3K9me2-containing nucleosomes, promoting their eviction/exchange from chromatin.

We found that dH1K27me2 regions are statistically enriched in several TFs binding motifs, some of which correspond to TFs that have been reported to associate with pericentromeric heterochromatin (i.e. Prod, GAGA and the PAX family TF eyegone (eyg)) (42–44). This observation was somehow unexpected since, although dH1K27me2 regions are enriched in TEs, no significant enrichment in TFs binding motifs identified in *D. melanogaster* TEs was observed (45). A similar enrichment of certain TFs binding sequences in heterochromatin has been reported in mice and a role in heterochromatin formation for Pax3 and Pax9 has been proposed (46). In flies, binding of TFs to pericentromeric regions is generally dynamic (42,44), accumulating at heterochromatin only in metaphase chromosomes, which is similar to dH1K27me2 that is restricted to pericentromeric regions in mitosis. These observations suggest a link between TFs binding and dH1K27me2.

In summary, here we have characterized K27me2 of *Drosophila* linker histone dH1 as a novel epigenetic modification that contributes to heterochromatin organization independently of H3K9 methylation. Interestingly, dH1K27me2 occurs within a short conserved sequence motif that has been reported to be methylated in some mammalian H1 variants (12,13), opening the possibility that the contribution of K27 methylation to heterochromatin organization is not constrained to *Drosophila*. Overall, our results highlight the potential of linker histones H1 PTMs as epigenetic regulators of chromatin structure and function. However, further work is required to identify enzymes regulating dH1K27 methylation since, unfortunately, all candi-
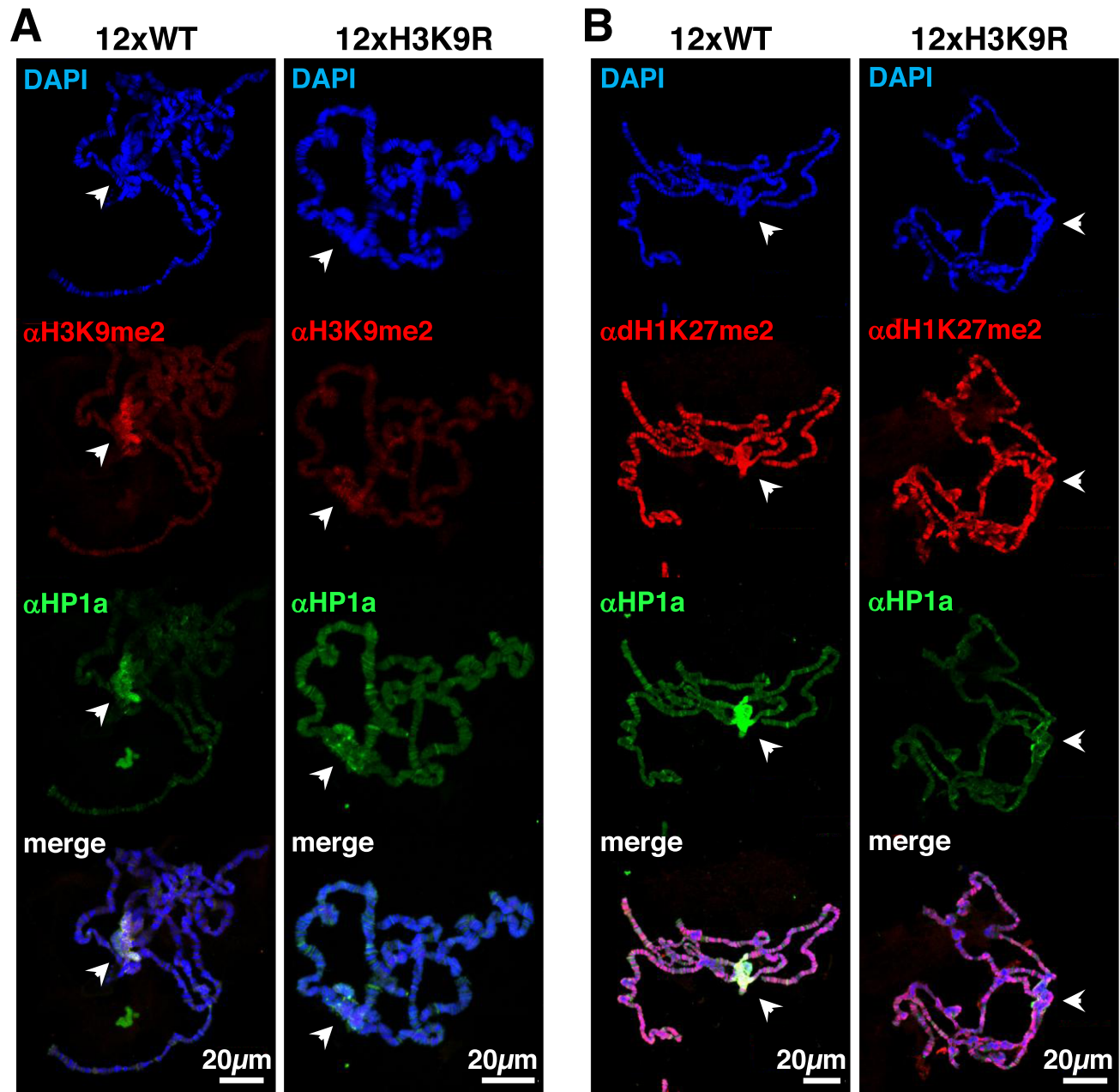
Figure 8. dH1K27me2 is independent of histone H3K9 methylation. (**A**) Immunostaining with αH3K9me2 (in red) and αHP1a (in green) of polytene chromosomes from flies carrying 12 copies of a wild-type WT (left) or a mutated H3K9R histone repeat (right) in front of a deficiency of the *HisC* locus. DNA was stained with DAPI (in blue). Arrowheads indicate the chromocenter. Scale bars correspond to 20μm. (**B**) As in A but stained with αdH1K27me2 (in red) and αHP1a (in green).

dates that we tested failed to show any significant contribution.

DATA AVAILABILITY

ChIPseq data are deposited at NCBI GEO (GSE167018, GSE127227). All other data are available on request.

SUPPLEMENTARY DATA

Supplementary Data are available at NAR Online.

REFERENCES

1. Fyodorov,D.V., Zhou,B.-R., Skoultchi,A.I. and Bai,Y. (2018) Emerging roles of linker histones in regulating chromatin structure and function. *Nat. Rev. Mol. Cell Biol.*, **19**, 193–206.
2. Kouzarides,T. (2007) Chromatin modifications and their function. *Cell*, **128**, 693–705.
3. Kharchenko,P.V., Alekseyenko,A.A., Schwartz,Y.B., Minoda,A., Riddle,N.C., Ernst,J., Sabo,P.J., Larschan,E., Gorchakov,A.A., Gu,T. *et al.* (2011) Comprehensive analysis of the chromatin landscape in *Drosophila melanogaster*. *Nature*, **471**, 480–485.
4. Filion,G.J., van Bemmel,J.G., Braunschweig,U., Talhout,W., Kind,J., Ward,L.D., Brugman,W., de Castro,I.J., Kerkhoven,R.M., Bussemaker,H.J. *et al.* (2010) Systematic protein location mapping reveals five principal chromatin types in *Drosophila* cells. *Cell*, **143**, 212–224.
5. Elgin,S.C.R. and Reuter,G. (2013) Position-Effect variegation, heterochromatin formation, and gene silencing in *Drosophila*. *Cold Spring Harb. Perspect. Biol.*, **5**, a017780.
6. Schotta,G., Lachner,M., Sarma,K., Ebert,A., Sengupta,R., Reuter,G., Reinberg,D. and Jenuwein,T. (2004) A silencing pathway to induce H3-K9 and H4-K20 trimethylation at constitutive heterochromatin. *Genes Dev.*, **18**, 1251–1262.
7. Kourmouli,N., Jeppesen,P., Mahadevhaiah,S., Burgoyne,P., Wu,R., Gilbert,D.M., Bongiorni,S., Prantera,G., Fanti,L., Pimpinelli,S. *et al.* (2004) Heterochromatin and tri-methylated lysine 20 of histone H4 in animals. *J. Cell Sci.*, **117**, 2491–2501.
8. Andrés,M., García-Gomis,D., Ponte,I., Suau,P. and Roque,A. (2020) Histone H1 post-translational modifications: update and future perspectives. *Int. J. Mol. Sci.*, **21**, 5941.
9. Pérez-Montero,S., Carbonell,A. and Azorín,F. (2015) Germline-specific H1 variants: the "sexy" linker histones. *Chromosoma*, **125**, 1–13.
10. Bayona-Feliu,A., Casas-Lamesa,A., Carbonell,A., Climent-Cantó,P., Tatarski,M., Pérez-Montero,S., Azorín,F. and Bernués,J. (2016) Histone H1: lessons from *Drosophila*. *Biochim. Biophys. Acta*, **1859**, 526–532.
11. Pérez-Montero,S., Carbonell,A., Morán,T., Vaquero,A. and Azorín,F. (2013) The embryonic linker histone H1 variant of *Drosophila*, dBigH1, regulates zygotic genome activation. *Dev. Cell*, **26**, 578–590.
12. Wisniewski,J.R., Zougman,A., Krüger,S. and Mann,M. (2007) Mass spectrometric mapping of linker histone H1 variants reveals multiple acetylation, methylations, and phosphorylation as well as differences between cell culture and tissue. *Mol. Cell. Proteomics*, **6**, 72–87.
13. Bonet-Costa,C., Vilaseca,M., Diema,C., Vujatovic,O., Vaquero,A., Omeñaca,N., Castejón,L., Bernués,J., Giralt,E. and Azorín,F. (2012) Combined bottom-up and top-down mass spectrometry analyses of the pattern of posttranslational modifications of *Drosophila melanogaster* linker histone H1. *J. Proteomics*, **75**, 4124–4138.
14. Clarkson,M. and Saint,R. (1999) A *His2AvDGFP* fusion gene complements a lethal *His2AvD* mutant allele and provides an in vivo marker for *Drosophila* chromosome behavior. *DNA Cell Biol.*, **18**, 457–462.
15. McKay,D.J., Klusza,S., Penke,T.J.R., Meers,M.P., Curry,K.P., McDaniell,S.L., Malek,P.Y., Cooper,S.W., Tatomer,D.C., Lieb,J.D. *et al.* (2015) Interrogating the function of metazoan histones using engineered gene clusters. *Dev. Cell*, **32**, 373–386.
16. Lloret-Llinares,M., Carré,C., Vaquero,A., de Olano,N. and Azorín,F. (2008) Characterization of *Drosophila melanogaster* JmjC+N histone demethylases. *Nucleic Acids Res.*, **36**, 2852–2863.
17. Bayona-Feliu,A., Casas-Lamesa,A., Reina,O., Bernués,J. and Azorín,F. (2017) Linker histone H1 prevents R-loop accumulation and genome instability in heterochromatin. *Nat. Commun.*, **8**, 283.
18. Li,W. and Godzik,A. (2006) Cd-hit: a fast program for clustering and comparing large sets of protein or nucleotide sequences. *Bioinformatics*, **22**, 1658–1659.
19. Font-Burgada,J., Rossell,D., Auer,H. and Azorín,F. (2008) *Drosophila* HP1c isoform interacts with zinc-finger proteins WOC and relative-of-WOC to regulate gene expression. *Genes Dev.*, **22**, 3007–3023.
20. Boguslawski,S.J., Smith,D.E., Michalak,M.A., Mickelson,K.E., Yehle,C.O., Patterson,W.L. and Carrico,R.J. (1986) Characterization of monoclonal antibody to DNA.RNA and its application to immunodetection of hybrids. *J. Immunol. Methods*, **89**, 23–30.
21. Blanch,M., Piñeyro,D. and Bernués,J. (2015) New insights for Drosophila GAGA factor in larvae. *R. Soc. Open Sci.*, **2**, 150011.
22. Piñeyro,D., Blanch,M., Badal,M., Kosoy,A. and Bernués,J. (2013) GAGA factor repression of transcription is a rare event but the negative regulation of *Trl* is conserved in *Drosophila* species. *Biochim. Biophys. Acta*, **1829**, 1056–1065.
23. Jamrich,M., Greenleaf,A.L. and Bautz,E.K. (1977) Localization of RNA polymerase in polytene chromosomes of *Drosophila melanogaster*. *Proc. Natl. Acad. Sci. U.S.A.*, **74**, 2079–2083.
24. Alfageme,C.R., Rudkin,G.T. and Cohen,L.H. (1976) Locations of chromosomal proteins in polytene chromosomes. *Proc. Natl. Acad. Sci. U.S.A.*, **73**, 2038–2042.
25. Lu,X., Wontakal,S.N., Emelyanov,A.V., Morcillo,P., Kovev,A.Y., Fyodorov,D.V. and Skoultchi,A.I. (2009) Linker histone H1 is essential for *Drosophila* development, the establishment of pericentric heterochromatin, and a normal polytene chromosome structure. *Genes Dev.*, **23**, 452–465.
26. Belyaeva,E.S., Andreyeva,E.N., Belyakin,S.N., Volkova,E.I. and Zhimulev,I.F. (2008) Intercalary heterochromatin in polytene chromosomes of *Drosophila melanogaster*. *Chromosoma*, **117**, 411–418.
27. Kaminker,J., Bergman,C., Kronmiller,B., Carlson,J., Svirskas,R., Patel,S., Frise,E., Wheeler,D.A., Lewis,S.E., Rubin,G.M. *et al.* (2002) The transposable elements of the Drosophila melanogaster euchromatin: a genomics perspective. *Genome Biol.*, **3**, 0084.0081–0084.0020.
28. Climent-Cantó,P., Carbonell,A., Tatarski,M., Reina,O., Bujosa,P., Font-Mateu,J., Bernués,J., Beato,M. and Azorín,F. (2020) The embryonic linker histone dBigH1 alters the functional state of active chromatin. *Nucleic Acids Res.*, **48**, 4147–4160.
29. Schotta,G., Ebert,A., Krauss,V., Fischer,A., Hoffman,J., Rea,S., Jenuwein,T., Dorn,R. and Reuter,G. (2002) Central role of Drosophila SU(VAR)3-9 in histone H3-K9 methylation and heterochromatin gene silencing. *EMBO J.*, **21**, 1121–1131.
30. Armstrong,R.L. and Duronio,R.J. (2019) Phasing in heterochromatin during development. *Genes & Dev.*, **33**, 379–381.
31. Seum,C., Reo,E., Peng,H., Rauscher,F.J., Spierer,P. and Bontron,S. (2007) Drosophila SETDB1 is required for chromosome 4 silencing. *PLos Genet.*, **3**, e76.
32. Tzeng,T.Y., Lee,C.H., Chan,L.W. and Shen,C.K. (2007) Epigenetic regulation of the Drosophila chromosome 4 by the histone H3K9 methyltransferase dSETDB1. *Proc. Natl. Acad. Sci. U.S.A.*, **104**, 12691–12696.
33. Haynes,K.A., Gracheva,E. and Elgin,S.C.R. (2007) A distinct type of heterochromatin within *Drosophila melanogaster* Chromosome 4. *Genetics*, **175**, 1539–1542.
34. Traverse,K.L. and Pardue,M.L. (1989) Studies of He-T DNA sequences in the pericentric regions of Drosophila chromosomes. *Chromosoma*, **97**, 261–271.
35. Méndez-Lago,M., Wild,J., Whitehead,S.L., Tracey,A., de Pablos,B., Rogers,J., Szybalski,W. and Villasante,A. (2009) Novel sequencing strategy for repetitive DNA in a Drosophila BAC clone reveals that the centromeric region of the Y chromosome evolved from a telomere. *Nucleic Acids Res.*, **37**, 2264–2273.
36. Piacentini,L., Fanti,L., Negri,R., Del Vescovo,V., Fatica,A., Altieri,F. and Pimpinelli,S. (2009) Heterochromatin Protein 1 (HP1a) positively regulates euchromatic gene expression through RNA transcript

association and interaction with hnRNPs in *Drosophila*. *PLoS Genet.*, **5**, e1000670.

37. Terrenoire,E., McRonald,F., Halsall,J.A., Page,P., Illingworth,R.S., Taylor,A.M.R., Davison,V., O'Neill,L.P. and Turner,B.M. (2010) Immunostaining of modified histones defines high-level features of the human metaphase epigenome. *Genome Biol.*, **11**, R110.

38. Misteli,T., Gunjan,A., Hock,R., Bustin,M. and Brown,D.T. (2000) Dynamic binding of histone H1 to chromatin in living cells. *Nature*, **408**, 877–861.

39. Phair,R.D. and Misteli,T. (2000) High mobility of proteins in the mammalian cell nucleus. *Nature*, **404**, 604–609.

40. Lu,X., Wontakal,S.N., Kavi,H., Kim,B.J., Guzzardo,P.M., Emelyanov,A.V., Xu,N., Hannon,G.J., Zavadil,J., Fyodorov,D.V. *et al.* (2013) Drosophila H1 regulates the genetic activity of heterochromatin by recruitment of Su(var)3-9. *Science*, **340**, 78–81.

41. Vujatovic,O., Zaragoza,K., Vaquero,A., Reina,O., Bernués,J. and Azorín,F. (2012) *Drosophila melanogaster* linker histone dH1 is required for transposon silencing and to preserve genome integrity. *Nucleic Acids Res.*, **40**, 5402–5414.

42. Platero,J.S., Csink,A.K., Quintanilla,A. and Henikoff,S. (1997) Changes in chromosomal localization of heterochromatin binding proteins during the cell cycle in Drosophila. *J. Cell Biol.*, **140**, 1297–1306.

43. Salvany,L., Requena,D. and Azpiazu,N. (2012) Functional association between eyegone and HP1a mediates wingless transcriptional repression during development. *Mol. Cell. Biol.*, **32**, 2407–2415.

44. Delattre,M., Spierer,A., Tonka,C.-H. and Spierer,P. (2000) The genomic silencing of position-effect variegation in Drosophila melanogaster: interaction between the heterochromatin-associated proteins Su(var)3-7 and HP1. *J. Cell Sci.*, **113**, 4253–4261.

45. Villanueva-Cañas,J.L., Horvath,V., Aguilera,L. and González,J. (2019) Diverse families of transposable elements affect the transcriptional regulation of stress-response genes in Drosophila melanogaster. *Nucleic Acids Res.*, **47**, 6842–6857.

46. Bulut-Karslioglu,A., Perrera,V., Scaranaro,M., de la Rosa-Velazquez,I.A., van de Nobelen,S., Shukeir,N., Popow,J., Gerle,B., Opravil,S., Pagani,M. *et al.* (2012) A transcription factor–based mechanism for mouse heterochromatin formation. *Nat. Struc. Mol. Biol.*, **19**, 1023–1030.